Diffusive impurity transport driven by trapped particle turbulence in tokamak plasmas

E. Gravier (iD), M. Lesur (iD), X. Garbet (iD), Y. Sarazin (iD), J. Médina, K. Lim, and M. Idouakass

View Online   Export Citation   CrossMark

ARTICLES YOU MAY BE INTERESTED IN

Diffusive impurity transport driven by trapped particle turbulence in tokamak plasmas

View Online   Export Citation   CrossMark

E. Gravier,[1] (iD) M. Lesur,[1] (iD) X. Garbet,[2] (iD) Y. Sarazin,[2] (iD) J. Médina,[1] K. Lim,[1] and M. Idouakass[1]

AFFILIATIONS

[1]IJL, UMR 7198 CNRS-Université de Lorraine, 54 000 Nancy, France
[2]CEA, IRFM, 13 108 Saint-Paul-lez-Durance, France

ABSTRACT

The diffusive impurity transport as a function of charge and mass numbers is investigated in ion driven or electron driven turbulence, in the limit of zero impurity temperature gradient. It is found that the impurity transport decreases slightly with increasing mass number and depends much more strongly on the charge number. Moreover, this transport depends on the nature of the instability that drives turbulence. The impurity flux due to Trapped Electron Mode (TEM) turbulence increases with the charge number Z. In contrast, it is found to decrease with Z when the Trapped Ion Mode (TIM) dominated. In order to explain these observations, the quasilinear flux is derived and is compared with the results obtained from the nonlinear simulations. Quasilinear theory qualitatively reproduces the gyrokinetic numerical observations.

Published under license by AIP Publishing. https://doi.org/10.1063/1.5107443

I. INTRODUCTION AND MODEL

In tokamak plasmas, all particles that are not electrons or do not contribute to the reaction of fusion are defined as impurities. For instance, argon or neon can be introduced in the plasma edge as impurity seeding used for tailoring the radiation profile near the plasma-facing components. The propagation of these particles into the plasma core can be problematic. Moreover, transport and accumulation of tungsten from the wall to the core can also be prohibitive, for concentrations as low as 3×10^{-5}.[1] In contrast, helium ash produced by the reactions of fusion must be transported from the core to the wall. Therefore, impurity accumulation in the plasma core must be avoided and impurity transport is an issue that needs to be understood. For example, the direction of this transport, i.e., inward or outward, can be predicted by neoclassical theory, depending on both the main ion density gradient and the temperature gradient. In addition, turbulence also contributes to impurity flux.

In this work, we focus on turbulence issues. The second and third terms on the RHS of the following equation, which denote the thermo-diffusive pinch and the curvature-driven pinch, respectively,

$$\Gamma = -D\frac{\partial n}{\partial r} + C_T\frac{\partial T}{\partial r} + C_P, \tag{1}$$

are neglected in our calculations, so that impurity transport Γ calculations only include diffusive transport [the first term on the RHS of Eq. (1), $\Gamma = -D\frac{\partial n}{\partial r}$]. Moreover, our model is collisionless, meaning that neoclassical transport is not taken into account. The expected

increasing importance of the turbulent transport of impurities in a reactor plasma motivates our study. Turbulent impurity transport is expected to have a larger weight in future reactor size plasmas than in present devices,[2] in which neoclassical transport is relatively higher. Isotopic effects (hydrogenic mass effects) on impurity transport have been studied,[3] but these investigations are limited to $Z = 2$–3, whereas we aim at covering a larger range. The dependence of impurity transport on the impurity species has been studied as well,[2,4–13] but without decoupling the impacts of Z and A or focusing on the peaking factor. In a previous paper,[14] we have shown how a large concentration of tungsten can change the nature of the turbulence in the case of active species. In the present article, we perform scalings for the impurity diffusion coefficients with the impurity charge and the mass numbers and with the TEM or trapped ion mode (TIM) driven modes, in the case where impurity concentrations do not affect the nature of the turbulence. Impurity turbulent fluxes are investigated via both gyrobounce-kinetic simulations and quasilinear theory. The gyrokinetic code we use is named TERESA (Trapped Element REduction in Semi Lagrangian Approach).[15] It should be noted that the results of nonlinear simulations are often compared with the results of the quasilinear theory, which is relevant because its estimations of turbulent fluxes in most cases remain in good agreement with nonlinear gyrokinetic simulations[16] as well as with experimental results,[17] despite crude simplifications, and even if, in some cases, discrepancies between nonlinear simulations and quasilinear predictions are observed.[2]

To complete this introduction and for the benefit of the reader, below, we summarize the main assumptions and equations of the

gyrokinetic model[14] needed to understand the new investigations and results described in the rest of this article. The reader can find further information in Refs. 14, 15, and 18–28.

The model is relevant for relatively low frequency modes, such as Trapped-Ion Modes (TIMs) and Trapped-Electron Modes (TEMs). TEM and TIM are instabilities that are characterized by frequencies ω on the order of ω_d, the precession frequency. The latter frequency is smaller than ω_b, the bounce frequency, which itself is smaller than the cyclotron frequency ω_c. Therefore, it is possible to gyroaverage and bounce-average the Vlasov equation, thus filtering out the fast cyclotron and bounce frequencies, and the small space scales ρ_c (gyroradius) and δ_b (banana width). These assumptions lead to a reduction of dimensionality, from 5D gyrokinetics to 4D gyrobounce-gyrokinetics. We consider an adiabatic response of the passing particles, and thus, our reduced model with trapped kinetic particles covers both TIM/TEM regimes simultaneously but precludes other instabilities such as Ion-Temperature-Gradient (ITG) or Electron-Temperature-Gradient (ETG) instabilities.

The Vlasov equation reads

$$\frac{\partial f_s}{\partial t} - [\mathcal{J}_{0,s}\phi, f_s]_{\alpha,\psi} + \frac{\Omega_d E}{Z_s}\frac{\partial f_s}{\partial \alpha} = 0, \quad (2)$$

where f_s is the gyrobounce-averaged particle distribution function. The subscript $s = i$, e, and z stands for the species considered (main ion, electron, or impurity), and ϕ is the plasma potential. E is the particle kinetic energy. $\alpha = \varphi - q\theta$, with φ being the toroidal angle, θ the poloidal angle, and q the safety factor. ψ is the magnetic flux, the function of the radius $\psi = 1$ stands for the core plasma and $\psi = 0$ for the plasma edge. Z_s is the charge number. $\Omega_d = \frac{Z_s \omega_{d,s}}{E}$, with $\omega_{d,s}$ being the toroidal precession frequency for the species s.[29] For the main ion species, we choose $\Omega_d = 1$, and we neglect the variation of Ω_d over the radius (Ω_d only depends on the sign of the charge).

The gyrobounce-averaging operator is written as

$$\mathcal{J}_{0,s} = \left(1 - \frac{E}{T_{0,s}}\frac{\delta_{b0,s}^2}{4}\partial_\psi^2\right)^{-1}\left(1 - \frac{E}{T_{0,s}}\frac{q^2\rho_{c0,s}^2}{4a^2}\partial_\alpha^2\right)^{-1}, \quad (3)$$

where $\rho_{c0,s}$ and $\delta_{b0,s}$ are the Larmor radius and the banana width (expressed in units of ψ) and $T_{0,s}$ is the equilibrium temperature at $\psi = 0$, normalized to an arbitrary reference temperature T_0. $\omega_0 = T_0/(eR_0^2 B_\theta)$ corresponds to the ion precession frequency at the reference temperature T_0 (time is normalized to ω_0), and $L_\psi = aR_0 B_\theta$ is the radial length of the simulation box in units of ψ. ψ is normalized to L_ψ.

The normalized quasineutrality constraint is written as

$$\frac{2}{\sqrt{\pi}}\sum_s\left(Z_s\mathcal{C}_s\int_0^\infty \mathcal{J}_{0,s}f_s E^{1/2}dE\right)$$
$$= C_{ad}\left(\phi - \varepsilon_\phi\langle\phi\rangle_\alpha\right) - C_{pol}\sum_s \mathcal{C}_s\tau_s Z_s^2 \Delta_s\phi, \quad (4)$$

with $\mathcal{C}_s = n_s/n_{0,e}$ being the concentration of the species s (n_s is the population density and $n_{0,e}$ the electron density at equilibrium), $C_{pol} = e\omega_0 L_\psi/T_0$, and $C_{ad} = C_{pol}\frac{1-f_T}{f_T}\sum_s(Z_s^2\mathcal{C}_s\tau_s)$, where f_T is the fraction of trapped particles and $\tau_s = T_0/T_{0,s}$. The Laplacian operator expresses the difference between the particle density and the gyrobounce-center density, corresponding to an effective polarization.

ε_ϕ is a control parameter which governs the response of the adiabatic passing particles. Regarding this response, the reader can find further information in Refs. 14, 25, and 30. Hereafter, only the case $\varepsilon_\phi = 0.3$ is considered.

In Sec. II, linear results and nonlinear simulations are presented. It is shown how impurities behave as a function of the mass and charge numbers. In Sec. III, the quasilinear impurity fluxes are derived and compared with nonlinear numerical results. Finally, a brief summary of the results along with a conclusion is given in Sec. IV.

II. IMPURITY TRANSPORT AS A FUNCTION OF THE CHARGE NUMBER AND THE MASS NUMBER

We choose to implement the equilibrium distribution function as follows:

$$F_{eq,s} = \frac{n_{0,s}}{T_{0,s}^{3/2}}\exp\left(-\frac{E}{T_{0,s}}\right)\left[1 + \left(\kappa_{n,s} + \left(\frac{E}{T_{0,s}} - \frac{3}{2}\right)\kappa_{T,s}\right)\psi\right]. \quad (5)$$

For electrons and main ions, $\kappa_{T,ei} = \frac{1}{T_{e,i}}\partial_\psi T_{e,i}$ have finite values. For impurities, we choose $\kappa_{T,Z} = 0$ so that no thermodiffusion will appear for impurity transport. $\kappa_{n,s}$ is defined as $\frac{1}{n_s}\partial_\psi n_s$. The curvature driven pinch is also neglected in this model since a Taylor expansion at $\psi = 0$ of a Maxwellian distribution yields

$$F_{eq,s}^* = F_{eq,s} - \frac{n_{0,s}}{T_{0,s}^{3/2}}\frac{e\Omega_d E}{T_{0,s}}\psi\exp\left(-\frac{E}{T_{0,s}}\right). \quad (6)$$

The latter term is responsible for the curvature-driven pinch and is neglected in Eq. (5). Therefore, impurity transport calculations only include diffusive transport. The transport across the magnetic field is therefore adequately characterized as diffusivity.

For the linear study, we use the linear dispersion derived in Ref. 14. It reads

$$D = 0 = C_n - \sum_s Z_s\mathcal{C}_s\tau_s\int_0^\infty J_{n,s}^2\frac{\kappa_{n,s} + \kappa_{T,s}\left(\xi_s - \frac{3}{2}\right)}{\frac{\Omega_d}{Z_s}\left(\xi_s - W_s\right)}e^{-\xi_s}\xi_s^{\frac{1}{2}}d\xi, \quad (7)$$

with

$$C_n = \frac{\sqrt{\pi}}{2}\left[C_{ad} + C_{pol}n^2\sum_s\mathcal{C}_s\tau_s Z_s^2\rho_{c0,s}^2 + C_{pol}k^2\sum_s\mathcal{C}_s\tau_s Z_s^2\delta_{b0,s}^2\right]. \quad (8)$$

Here, $\xi = \frac{E}{T_{0,s}}$, $W_s = \frac{Z_s\omega}{n\Omega_d T_{0,s}}$, n is the mode number in the α-direction, $k = \pi$ is the most unstable radial mode, and ω is the complex mode frequency. This dispersion relation will be solved to find the growth rates and real frequencies of the TEM and TIM instabilities for two different cases that we investigate in this paper. For linearly solving Eq. (7), we scan the (ω_r, ω_i) plane, searching for values of ω such that the RHS of Eq. (7) vanishes within machine precision. For this purpose, a method that finds the minimum of a scalar function of several variables, starting in an initial state, and uses the simplex search method[31] is used. Actually, we start the scan from several initial values in the (ω_r, ω_i) plane in order to get all the possible roots. Among these solutions, one finds the couple (ω_r, ω_i) for which the instability growth rate ω_i is maximum. We simultaneously look at the region where ω_r is negative (TEM instability) and the region where ω_r is positive (TIM instability). We retain the maximum of ω_i for each of the two regions.

TABLE I. Main parameters used for the linear study and nonlinear simulations. The subscripts D, e, and Z stand for deuterium, electron, and impurities, respectively.

$\mathscr{C}_D$	$\mathscr{C}_e$	$\mathscr{C}_Z$	$\kappa_{n,D}$	$\kappa_{n,e}$	$\kappa_{n,Z}$	$\frac{T_{0_D,Z}}{T_{0,e}}$
0.9964	1.0	10^{-5}	0.1	0.099604	-1	1.0

Here and in the remainder of this paper, we consider a plasma composed of deuterium as the main ion species, electrons, and impurity species. In our calculations and simulations, all species are considered as active species, meaning that each species is described by its own distribution function and each species is taken into account in the quasineutrality constraint.

We choose five different simulated impurities with the same mass number ($A = 20$) but with 5 different charge numbers $Z = 2, 4, 8, 10,$ and 12. Regarding the A-dependence, another set of simulations is considered with the same charge number ($Z = 4$) but with 5 different mass numbers $A = 10, 30, 50, 70,$ and 90 in order to cover the same $\sqrt{A}/Z$ range as in the case of the Z-dependence. Other parameters used as inputs for the linear code and the nonlinear code are given Tables I–III. Species concentrations and density gradients are chosen according to quasineutrality, assuming that $n_{0,e} = 1$, $\kappa_{n,D} = 0.1$, $\mathscr{C}_Z = 10^{-5}$, and $\kappa_{n,Z} = -1$ for all impurities. The minus sign for $\kappa_{n,Z}$ means that the impurity density is larger at the plasma edge than at the plasma core, according to the fact that main impurities come from the wall. It should be noted that the results presented hereafter do not depend on the sign of $\kappa_{n,Z}$ and the plus sign could have been chosen. Other quantities from Table I are evaluated according to quasineutrality

$$\sum_s Z_s \mathscr{C}_s = 0, \tag{9}$$

which also leads to a constraint on $\kappa_{n,s}$,

$$\sum_s Z_s \mathscr{C}_s \kappa_{n,s} = 0. \tag{10}$$

The two different cases investigated in this paper are now presented.

The first one corresponds to $\partial_\psi T_D = 0.135$ and $\partial_\psi T_e = 0.18$. The dispersion relation [Eq. (7)] is numerically solved, and TEMs are found to be more unstable than TIM. This case is referred to as the

TEM case (Fig. 1). For these temperature gradients, the most unstable mode is $n = 74$, the instability growth rate is $\gamma = 28.4\ \omega_0$, and the real frequency $\omega_r = -68.4\ \omega_0$. In this case and with the ITER parameters, it should be noted that the order of magnitude of ω_r/ω_b is about 0.2 for deuterium and 0.005 for electrons. Thus, even if ω_r is much less than ω_b in the case of electrons, for deuterium ions, the condition of the mode frequency lower than the bounce frequency is less safely met. Nevertheless, with different electron/ion mass ratios leading to lower modes and smaller ω_r/ω_b, the results and the trends presented hereafter are very similar.

For the second case, $\partial_\psi T_D = 0.18$ and $\partial_\psi T_e = 0.135$. The dispersion relation is numerically solved, and TIMs are found to be more unstable than TEM. This case will be referred to as the TIM case (Fig. 2). For these temperature gradients, the most unstable mode is $n = 60$, the instability growth rate is $\gamma = 23.4\ \omega_0$, and the real frequency is $\omega_r = 56.9\ \omega_0$.

The results of the nonlinear simulations are now presented. A semi-Lagrangian method for the numerical resolution of the Vlasov equation is used.[32] These simulations have been performed with $N_\psi = 256$, $N_\alpha = 1024$, and $N_E = 192$. The numerical simulations are done using a thermal and density bath as boundary conditions: the temperature and density are fixed at $\psi = 0$ and $\psi = 1$. Dirichlet boundary conditions are imposed on the potential. The simulation parameters correspond to a radial box size of 166 Deuterium Larmor radii. First, we noticed (not shown in this paper) that for both cases, the most unstable modes displayed by the nonlinear TERESA simulations in the linear phase correspond to the linear growth rates given by the linear analysis, as well as the direction of propagation, along the α-direction for TIM instabilities and in the opposite direction for TEM instabilities. Then, in the nonlinear state, the fastest growing modes couple to the other eigenmodes, driving them up to the saturation level.

In order to evaluate impurity transport, while smoothing out fast turbulent fluctuations, we plot the cumulative flux along the ψ-direction (meaning along the radial direction) given by

$$\Gamma_{cumul} = \int_0^t \Gamma(t^*)dt^*, \tag{11}$$

with[21]

$$\Gamma(t) = -\frac{2}{\sqrt{\pi}} \int_0^{2\pi} d\alpha \int_0^\infty f \partial_\alpha (\mathcal{J}\phi) E^{1/2} dE. \tag{12}$$

TABLE II. Larmor radii used for the linear study and nonlinear simulations for deuterium (D), electrons (e), and impurities (Z). The values of the Larmor radii are at the thermal velocity, and the approximation of constant orbit widths is used.

$\rho_{c,D}$	$\rho_{c,e}$	$\rho_{c,Z=2}$	$\rho_{c,Z=4}$	$\rho_{c,Z=8}$	$\rho_{c,Z=10}$	$\rho_{c,Z=12}$
6×10^{-3}	10^{-4}	9.49×10^{-3}	4.74×10^{-3}	2.38×10^{-3}	1.90×10^{-3}	1.58×10^{-3}

TABLE III. Banana widths used for the linear study and nonlinear simulations, for deuterium (D), electrons (e), and impurities (Z). The values of the banana widths are at the thermal velocity, and the approximation of constant orbit widths is used.

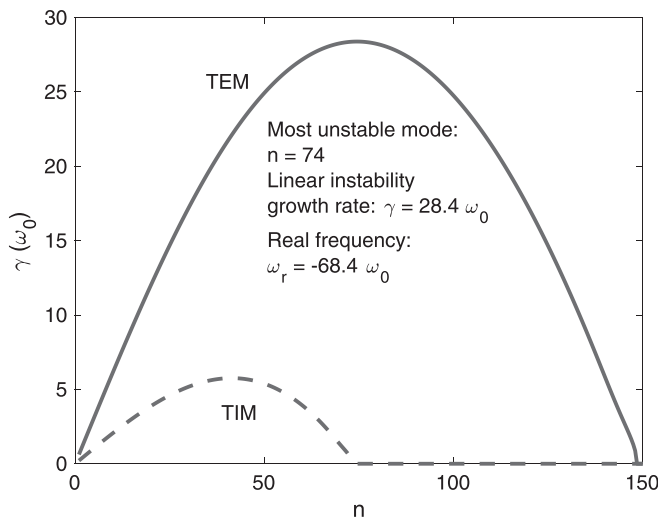| $\delta_{b,D}$	$\delta_{b,e}$	$\delta_{b,Z=2}$	$\delta_{b,Z=4}$	$\delta_{b,Z=8}$	$\delta_{b,Z=10}$	$\delta_{b,Z=12}$
6×10^{-2}	10^{-3}	9.49×10^{-2}	4.74×10^{-2}	2.37×10^{-2}	1.90×10^{-2}	1.58×10^{-2}

FIG. 1. Instability growth rates plotted against the mode number n, in the case $\partial_\psi T_e = 0.18$ and $\partial_\psi T_D = 0.135$, for TEM (solid line) and TIM (dotted line). For these temperature gradients, the most unstable mode $n = 74$ is a trapped electron mode (TEM).

A. Trapped electron mode case

We focus on the TEM case. The results regarding the Z-dependence are presented in Fig. 3. First, a linear phase is observed, followed by the saturation phase, at about $t = 0.6\,\omega_0^{-1}$. The system reaches a nearly steady state from $t = 0.8\,\omega_0^{-1}$. Then, the cumulative flux increases almost linearly, meaning that impurity particle flux is nearly constant. The slopes are determined from $t = 0.8$ to $t = 1.1\,\omega_0^{-1}$, and we can then evaluate the impurity flux Γ_Z. As we assume a pure diffusive transport, the global diffusion coefficient is given by
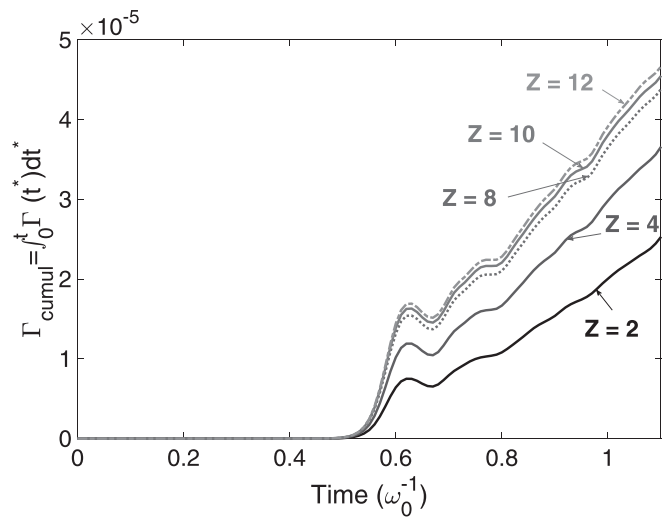

FIG. 3. Impurity cumulative flux $\int_0^t \Gamma(t^*)dt^*$ plotted against time in the case of a TEM turbulence. Different charge numbers are considered, with the same mass number $A = 20$. The higher charge impurity has larger impurity flux.

$$D_Z = -\frac{\Gamma_Z}{\partial_\psi n_Z}. \tag{13}$$

The diffusion coefficients for the TEM case are presented in Fig. 4. The diffusion coefficient D_{TEM} is plotted against the impurity charge number Z. The error bars correspond to the uncertainty in the determination of the slopes from Fig. 3. We observe in that case that the diffusion coefficient increases with the charge number. It should be noted that this trend is always observed when TEMs are the main instabilities and even if parameters are very different, for instance, if
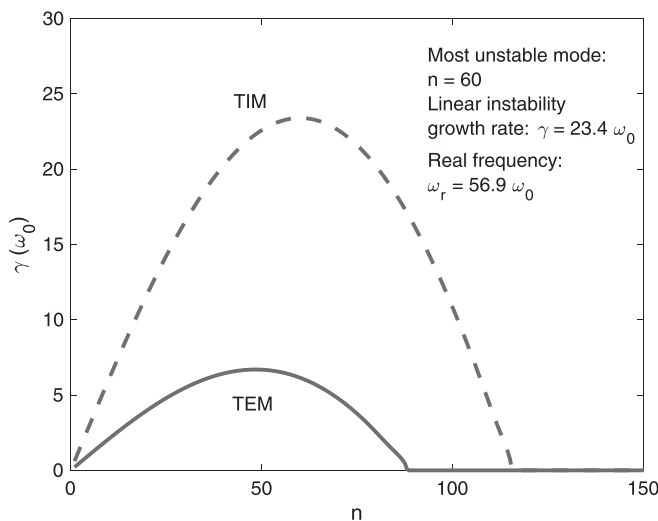

FIG. 2. Instability growth rates plotted against the mode number n, in the case $\partial_\psi T_e = 0.135$ and $\partial_\psi T_D = 0.18$, for TEM (solid line) and TIM (dotted line). For these temperature gradients, the most unstable mode $n = 60$ is a trapped ion mode (TIM).
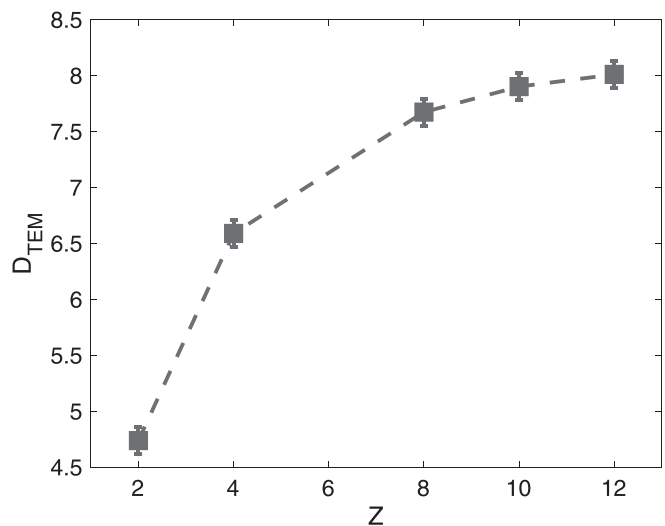

FIG. 4. Impurity diffusion D_{TEM} coefficient plotted against the impurity charge number Z in the case of TEM turbulence. The mass number is $A = 20$. The coefficient is calculated from Fig. 3, for $0.8 < t < 1.1$. The higher charge impurity has a larger diffusion coefficient.

we choose Larmor radii and banana widths such that the main unstable modes are much smaller (about $n = 10$ for instance). Moreover, other simulations have been performed with ε_ϕ greater than 0.3. In that case, zonal flows are stronger. The diffusion coefficient still increases with the charge number, but the diffusion coefficients are smaller, as expected when zonal flows are stronger (zonal flows are structures perpendicular to the radial direction which improves plasma confinement).

Nevertheless, we observe that impurity transport becomes roughly independent of impurity charge at high impurity charges, as observed in other studies.[2]

Finally, another important result is that this transport depends weakly on the mass number A of the species. Additional simulations have been carried out for five impurities with Z constant and different values of A. We performed simulations with $Z = 4$ and $A = 10, 30, 50, 70, 90$ in order to cover approximatively the same domain in $\sqrt{A}/Z$ as for the study of the Z-dependence (Fig. 5). The variation in A of the impurity diffusion coefficient is about 60% smaller than that in Z, for the same $\sqrt{A}/Z$ range, and is found to decrease with A.

B. Trapped ion mode case

Then, we consider the TIM case. The results regarding the Z-dependence are presented in Fig. 6. First, a linear phase is observed, followed by the saturation phase, at about $t = 0.75\,\omega_0^{-1}$. The system reaches a nearly steady state from $t = 1.0\,\omega_0^{-1}$. Then, the cumulative flux increases linearly, meaning that impurity particle flux is almost constant. The slopes are determined from $t = 1.0$ to $t = 1.55\,\omega_0^{-1}$, and then, as in the TEM case, we evaluate the impurity flux Γ_Z and the diffusion coefficients.

The diffusion coefficients D_{TIM} for the TIM case are presented in Fig. 7. The diffusion coefficient D_{TIM} is plotted against the impurity
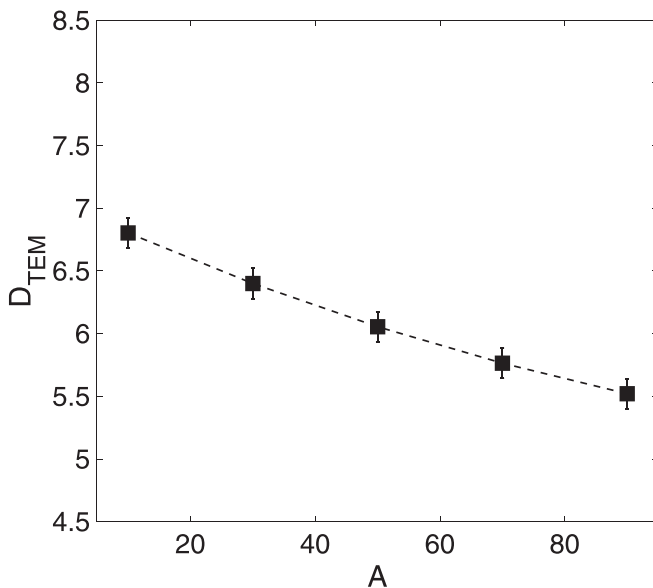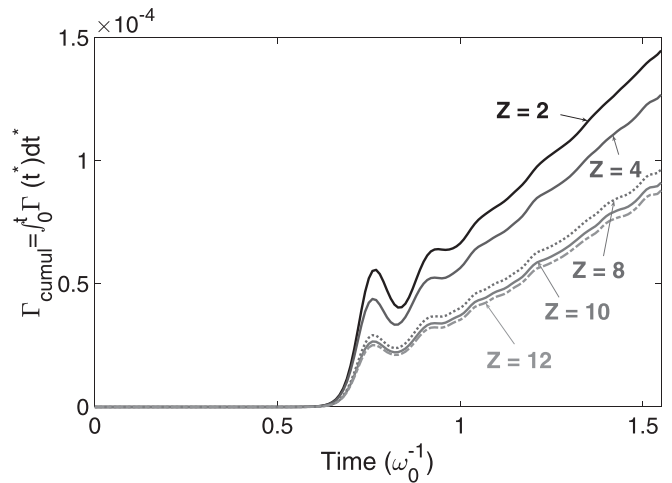

FIG. 6. Impurity cumulative flux $\int_0^t \Gamma(t^*)dt^*$ plotted against time in the case of a TIM turbulence. Different charge numbers are considered, with the same mass number $A = 20$. The higher charge impurity has smaller impurity flux.

charge number Z. The error bars correspond to the uncertainty in the determination of the slopes in Fig. 6. We observe in that case that the diffusion coefficient decreases with the charge number. It should be noted that this trend is always observed when TIMs are the main instabilities, even if plasma parameters are very different. The different scaling of the diffusion coefficient with Z will be shown in Sec. III to be related to a drift resonance.

Nevertheless, as in the TEM case, we observe that impurity transport becomes roughly independent of impurity charge at high impurity charge numbers.
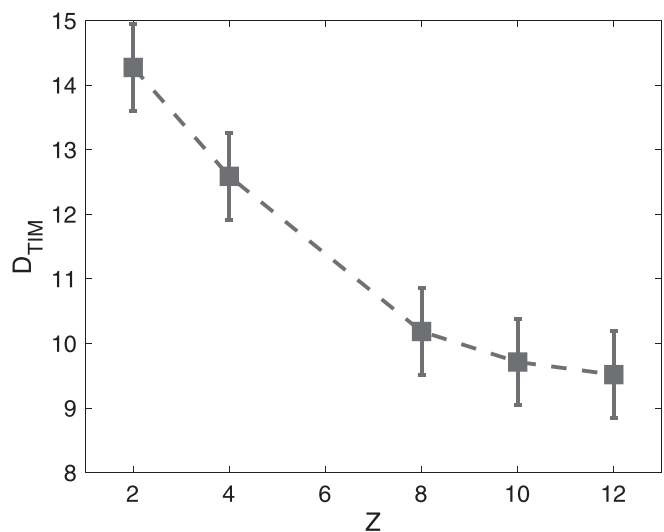

FIG. 5. Impurity diffusion D_{TEM} coefficient plotted against the mass number A in the case of TEM turbulence. The charge number is $Z = 4$. The coefficient depends more weakly on A than on Z (about 60%, the same scale as in Fig. 5 is used in ordinates in order to compare both the results).

FIG. 7. Impurity diffusion coefficient D_{TIM} plotted against the impurity charge number Z in the case of TIM turbulence. The mass number is $A = 20$. The coefficient is calculated from Fig. 6, for $1.07 < t < 1.55$. The higher charge impurity has a smaller diffusion coefficient.
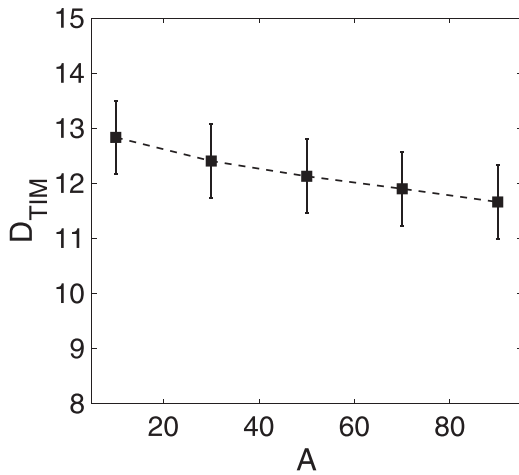
FIG. 8. Impurity diffusion D_{TIM} coefficient plotted against the mass number A in the case of TIM turbulence. The charge number is $Z = 4$. The coefficient depends more weakly on A than on Z (about 80%, the same scale as in Fig. 8 is used in ordinates in order to compare both the results).

As in the TEM case, another important result is that this transport depends weakly on the mass number A of the species. Simulations have been performed for five impurities with Z constant and different values of A. Again, we also performed simulations with $Z = 4$ and $A = 10, 30, 50, 70, 90$ in order to cover approximatively the same domain in $\sqrt{A}/Z$ (Fig. 8). The variation in A of the impurity diffusion coefficient is about 80% smaller than that in Z, for the same $\sqrt{A}/Z$ range, and is found to decrease with A.

C. Conclusion of the numerical simulations

From these results, we can conclude that in the case of turbulence driven by trapped particles, the impurity diffusive transport depends weakly on the mass number but depends mainly on the charge number. Moreover, this transport depends on the nature of the instability that drives turbulence: the diffusion coefficient is found to increase with Z in the case of TEM turbulence, while the diffusion coefficient is found to decrease with Z in the TIM dominated case.

We noticed that the change in flux regimes arises from the phase shifts between the density and potential fluctuations. These phase-shifts increase with Z in the case of TEM turbulence, while they come down with Z in the case of TIM turbulence.

In order to explain these observations, in Sec. III, a quasilinear calculation of impurity transport is derived from the TERESA model and comparisons with the numerical simulations are presented.

III. COMPARISON BETWEEN NUMERICAL SIMULATIONS AND THEORETICAL PREDICTIONS

In this section, the out of phase part of the distribution function to potential fluctuations is derived from the eigenmodes, and the quasilinear particle fluxes are determined, taking the power spectrum of the plasma potential fluctuations and the gradient parameters from TERESA simulation as input. Then, the comparisons between the

theoretically predicted impurity flux and the nonlinear impurity transport simulations are presented.

The banana-center distribution function f of one species (here, we consider an impurity species, and the subscript s is dropped) obeys the Vlasov equation

$$\frac{\partial f}{\partial t} - [\mathcal{J}\phi, f] + \frac{\Omega_d E}{Z}\frac{\partial f}{\partial \alpha} = 0, \tag{14}$$

with

$$[\mathcal{J}\phi, f] = \frac{\partial \mathcal{J}\phi}{\partial \alpha}\frac{\partial f}{\partial \psi} - \frac{\partial f}{\partial \alpha}\frac{\partial \mathcal{J}\phi}{\partial \psi}. \tag{15}$$

We assume that

$$f = f_0(E, t) + f_1 + f_2 + \cdots, \tag{16}$$

with $f_0(E, t)$ being the slowly evolving background distribution that changes due to the effects of the unstable waves, with $\frac{1}{f_0}\frac{\partial f_0}{\partial t} \ll \gamma_k$, where γ_k are the linear growth rates of the unstable waves. $f_{n \geq 1}$ are the small magnitude high frequency perturbations, of order ε^n, with $\varepsilon \ll 1$.

Quasilinear theory assumes that the amplitudes are still small enough that frequency and instantaneous growth rates of the modes are all adequately described by the linear theory. The linear theory yields

$$\frac{\partial f_1}{\partial t} - \frac{\partial \mathcal{J}\phi_1}{\partial \alpha}\frac{\partial f_0}{\partial \psi} + \frac{\Omega_d E}{Z}\frac{\partial f_1}{\partial \alpha} = 0. \tag{17}$$

Moreover, quantities with subscripts $n \geq 1$ are waves and therefore have spatial averages over α values which vanish ($\langle . \rangle = \frac{1}{2\pi}\int_\alpha . d\alpha$), so that Eq. (14), combined with Eq. (17), averaged over α, and neglecting terms with an order higher than 2, is written as

$$\frac{\partial f_0}{\partial t} = \frac{\partial}{\partial \psi}\left\langle f_1 \frac{\partial \mathcal{J}\phi_1}{\partial \alpha}\right\rangle. \tag{18}$$

The RHS term can be explicitly calculated by expressing the perturbations as a sum over spatial Fourier modes [$\phi_1(\alpha, t)$ $= \sum_n \phi_n e^{in\alpha}e^{-i\omega_n t}$, and the same for f_1] and by using Eq. (17) to get f_n as a function of ϕ_n, with f_n and ϕ_n being the amplitudes of the mode n of the perturbation. Assuming the developed distribution function (5) with $\kappa_T = 0$ (no thermodiffusion for impurities), the relationship between f_n and ϕ_n then is written as

$$f_n = \frac{\kappa_n}{\frac{\Omega_d}{Z}E - \frac{\omega_n}{n}}F_{eq_{\psi=0}}\mathcal{J}\phi_n, \tag{19}$$

and Eq. (18) yields

$$\frac{\partial f_0}{\partial t} - \frac{\partial}{\partial \psi}\left(\sum_n |n\mathcal{J}\phi_n|^2 \kappa_n F_{eq_{\psi=0}}\frac{\gamma_n}{(n\frac{\Omega_d}{Z}E - \omega_{r,n})^2 + \gamma_n^2}\right) = 0, \tag{20}$$

where the sum is over linearly unstable modes only, with $\omega_n = \omega_{r,n} + i\gamma_n$, and $\omega_{r,n}$ and γ_n are the real frequency and the linear growth rate of the mode n, respectively, determined by the linear dispersion relation [Eq. (7)].

By integrating this last equation over energy E (the Jacobian is proportional to $E^{1/2}dE$), we obtain

$$\frac{\partial n_0}{\partial t} + \frac{\partial \Gamma_\psi}{\partial \psi} = 0, \tag{21}$$

with Γ_ψ being the impurity transport in the radial direction

$$\Gamma_\psi = -\kappa_n \int_E \sum_n |n\mathcal{J}\phi_n|^2 \frac{\gamma_n}{\left(\omega_{r,n} - n\frac{\Omega_d}{Z}E\right)^2 + \gamma_n^2} F_{eq_{\psi=0}} E^{1/2} dE. \tag{22}$$

Both γ_n and $\omega_{r,n}$ have very weak dependency on both Z and A since in this article, only trace impurities are considered, and therefore, turbulence is governed by electrons and main ions: The more direct impacts of impurity species in the Poisson equation are negligible for $Z_s^2 \mathcal{C}_s \ll 1$.[33] Therefore, from this last equation (22), we can see that the radial impurity flux depends on the charge number Z as expected but depends weakly on the mass number. Indeed, the impurity mass only impacts the gyrobounce-averaging operator, where the Larmor radius and the banana width are proportional to $\sqrt{A}/Z$ [Eq. (3)]. But this A-dependence of the gyrobounce-averaging operator is weak and does not depend on the sign of ω_r and the nature of the instability. Regarding the A-dependence, the impurity flux is expected to decrease as A increases, in both TEM and TIM cases. These results are in agreement with the numerical simulations.

This expression [Eq. (22)] can be further evaluated and we now consider the two different cases. The real frequencies $\omega_{r,n}$ and the linear growth rates γ_n are needed and determined by solving the linear dispersion relation [Eq. (7)]. The saturation level of the plasma potential is given by nonlinear simulations.

A. Trapped electron mode case

For TEM instabilities, $\frac{\omega_{r,n}}{n} < 0$, and therefore, $\left(\frac{\omega_{r,n}}{n} - \frac{\Omega_d}{Z}E\right)$ is always negative. We evaluate the integral $\Gamma_{\psi,TEM}$ using Eq. (22), and we compare the results $D_{QL_{TEM}} = -\Gamma_{\psi,TEM}/\partial_\psi n$ with those given by the nonlinear simulations (Fig. 4).

As we focus on the Z dependence, we adjust the choice of $|\phi_n| = 0.05$ to get the best reasonable agreement between the two curves, but it should be noted that this choice is in qualitative agreement with the amplitude of the modes given by the nonlinear TERESA simulations. The results are presented in Fig. 9. The dotted line corresponds to the nonlinear results already presented in Fig. 4, and the solid line is $D_{QL_{TEM}}$. As expected, the quasilinear diffusion coefficient is found to increase as a function of the impurity charge number. Here, the quasilinear flux is evaluated by summing over the n components of the Fourier decomposition in α. But it should be noted that the quasilinear calculations yield almost the same results for Γ_ψ whatever the method we used: taking into account only the most unstable mode or considering the sum over all unstable modes.

We remark that in that case, there is very good agreement between the quasilinear theory and the results of the numerical simulations, despite the strong assumptions made in the quasilinear calculations.

B. Trapped ion mode case

For TIM instabilities, $\frac{\omega_{r,n}}{n} > 0$, and therefore, resonance is possible; by assuming γ_n small enough, the Lorentzian can be approximated in the resonant portion by
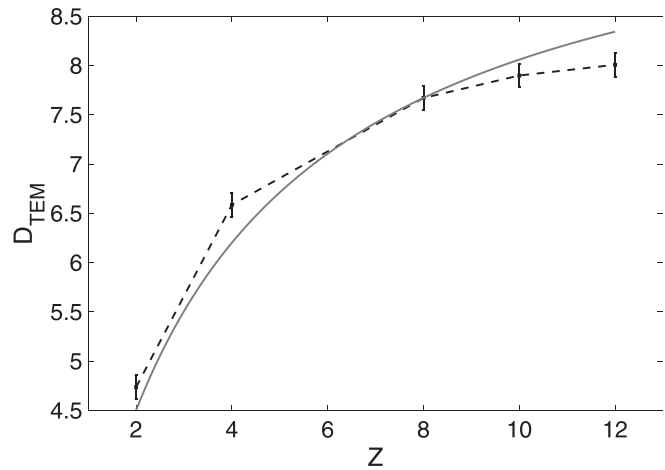

FIG. 9. Impurity diffusion coefficient D_{TEM} plotted against the impurity charge number Z in the case of TEM turbulence. The dotted line corresponds to the nonlinear results already presented in Fig. 4, and the solid line is $D_{QL_{TEM}}$. As in the numerical simulations, the quasilinear diffusion coefficient is also found to increase as a function of the impurity charge number.

$$\frac{\gamma_n}{\left(\omega_{r,n} - n\frac{\Omega_d}{Z}E\right)^2 + \gamma_n^2} \sim \pi\delta\left(\omega_{r,n} - n\frac{\Omega_d}{Z}E\right). \tag{23}$$

The integration over energy yields

$$\Gamma_{\psi,TIM} = -\kappa_n \frac{n_0}{T_0^{3/2}} \sum_n |n\mathcal{J}\phi_n|^2 \pi \left(\frac{Z}{n\Omega_d}\right)^{3/2} \omega_{r,n}^{1/2} e^{-\frac{Z\omega_{r,n}}{n\Omega_d T_0}}. \tag{24}$$

It should be noted that even though the delta-function expansion condition $\gamma_n/\omega_{r,n} \ll 1$ does not apply well in this case ($\gamma_n/\omega_{r,n} = 0.41$
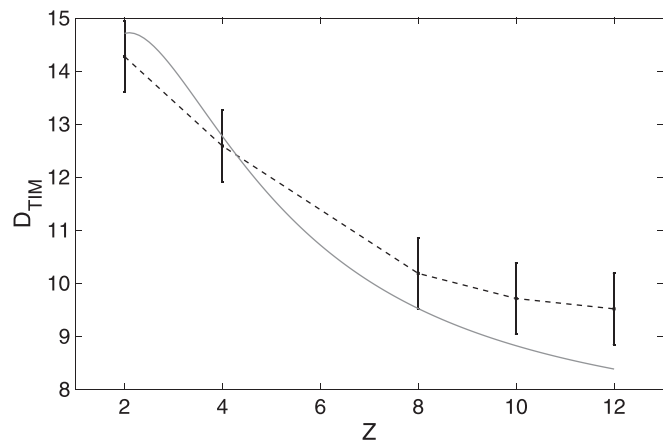

FIG. 10. Impurity diffusion coefficient D_{TIM} plotted against the impurity charge number Z in the case of TIM turbulence. The dotted line corresponds to the nonlinear results already presented in Fig. 7, and the solid line is $D_{QL_{TIM}}$. The quasilinear diffusion coefficient is also found to decrease as a function of the impurity charge number, and the nonlinear flux and the quasilinear prediction are in qualitative agreement.

for the most unstable mode), the monotonically decreasing dependence on Z is still captured by Eq. (24).

But in order to limit the sources of discrepancies, we evaluate numerically the quasilinear diffusion coefficients $D_{QL_{TIM}} = -\Gamma_{\psi,TIM}/\partial_\psi n$ using Eq. (22) for $\Gamma_{\psi,TIM}$ and compare them with those given by the nonlinear simulations (Fig. 7). In this case, to avoid small values of $\gamma_n/\omega_{r,n}$, only the most unstable mode $n = 60$ is retained in the calculation. The results are presented in Fig. 10. The dotted line corresponds to the nonlinear results already presented in Fig. 7, and the solid line is $D_{QL_{TIM}}$. The quasilinear diffusion coefficient monotonically decreases as a function of the impurity charge number, and the nonlinear flux and the quasilinear prediction are in qualitative agreement. The maximum discrepancy is equal to about 15%. This result is not totally surprising considering the fact that nonlinear simulations and quasilinear predictions are not always similar[34] for the TERESA model.

For the study presented in this article, we can therefore conclude that both trends of turbulent impurity transport with increasing Z (increasing in the TEM case and decreasing in the TIM case) are consistent with quasilinear theory.

IV. CONCLUSION

In the present article, the impact of the charge and mass numbers on impurity turbulent fluxes has been investigated via both gyrobounce-kinetic simulations and quasilinear theory. All the results shown in this work are from simulations and calculations carried out using the TERESA model. The trapped particles are treated kinetically, while the passing particles respond adiabatically. The model is meant to investigate fundamental mechanisms and trends, rather than provide realistic quantitative predictions for tokamaks. The simulation parameters correspond to a radial box size of 166 deuterium Larmor radii.

While impurity transport depends weakly on the impurity mass, it is found that it is mainly dependent on the impurity charge number. Moreover, it is found that impurity transport depends on the background turbulence: Impurity flux due to TEM turbulence increases with Z, while it decreases with Z in the case of TIM turbulence. In contrast, for the A-dependence, we observe that the diffusion coefficient decreases weakly with increasing A in both TEM and TIM cases.

The methodology of quasilinear theory has been shown to be applicable in this case as it determines the relative strength of the impurity ion transport and qualitatively explains the results obtained from the nonlinear numerical simulations.

REFERENCES

[1]T. Putterich, R. Neu, R. Dux, A. D. Whiteford, M. G. O'Mullane, and H. P. Summers, and the ASDEX Upgrade Team Nucl. Fusion **50**, 025012 (2010).

[2]C. Angioni, R. Bilato, F. J. Casson, E. Fable, P. Mantica, T. Odstrcil, and M. Valisa, ASDEX Upgrade Team and JET Contributors. Nucl. Fusion **57**, 022009 (2017).

[3]W. Guo, L. Wang, and G. Zhuang, Phys. Plasmas **23**, 112301 (2016).

[4]H. Nordman, A. Skyman, P. Strand, C. Giroud, F. Jenko, F. Merz, V. Naulin, and T. Tala, and the JET-EFDA Contributors. Plasma Phys. Cont. Fusion **53**, 105005 (2011).

[5]H. Du, Z. X. Wang, J. Q. Dong, and S. F. Liu, Phys. Plasmas **21**, 052101 (2014).

[6]N. Bonanomi, P. Mantica, C. Giroud, C. Angioni, P. Manas, and S. Menmuir, and JET Contributors. Nucl. Fusion **58**, 036009 (2018).

[7]S. Futatani, W. Horton, S. Benkadda, I. O. Bespamyatnov, and W. L. Rowan, Phys. Plasmas **17**, 072512 (2010).

[8]C. Angioni, R. M. McDermott, E. Fable, R. Fischer, T. Putterich, F. Ryter, and G. Tardini, and the ASDEX Upgrade Team. Nucl. Fusion **51**, 023006 (2011).

[9]F. J. Casson, C. Angioni, E. A. Belli, R. Bilato, P. Mantica, T. Odstrcil, T. Putterich, M. Valisa, L. Garzotti, C. Giroud et al., Plasma Phys. Controlled Fusion **57**, 014031 (2015).

[10]T. Fulop and H. Nordman, Phys. Plasmas **16**, 032306 (2009).

[11]A. Skyman, L. Fazendeiro, D. Tegnered, H. Nordman, J. Anderson, and P. Strand, Nucl. Fusion **54**, 013009 (2014).

[12]Y. Camenen, A. G. Peeters, C. Angioni, F. J. Casson, W. A. Hornsby, A. P. Snodin, and D. Strintzi, Phys. Plasmas **16**, 012503 (2009).

[13]P. Manas, W. A. Hornsby, C. Angioni, Y. Camenen, and A. G. Peeters, Plasma Phys. Controlled Fusion **59**, 035002 (2017).

[14]M. Idouakass, E. Gravier, M. Lesur, J. Médina, T. Réveillé, T. Drouot, X. Garbet, and Y. Sarazin, Phys. Plasmas **25**, 062307 (2018).

[15]T. Drouot, E. Gravier, T. Reveille, A. Ghizzo, P. Bertrand, X. Garbet, Y. Sarazin, and T. Cartier-Michaud, Eur. Phys. J. D **68**, 280 (2014).

[16]F. Jenko, T. Dannert, and C. Angioni, Plasma Phys. Controlled Fusion **47**, B195 (2005).

[17]C. Bourdelle, J. Citrin, B. Baiocchi, A. Casati, P. Cottier, X. Garbet, and F. Imbeaux, and JET Contributors, Plasma Phys. Cont. Fusion **58**, 014036 (2016).

[18]M. Tagger, G. Laval, and R. Pellat, Nucl. Fusion **17**, 109 (1977).

[19]H. Biglari, P. H. Diamond, and P. W. Terry, Phys. Fluids **31**, 2644 (1988).

[20]G. Depret, X. Garbet, P. Bertrand, and A. Ghizzo, Plasma Phys. Controlled Fusion **42**, 949 (2000).

[21]Y. Sarazin, V. Grandgirard, E. Fleurence, X. Garbet, Ph. Ghendrih, P. Bertrand, and G. Depret, Plasma Phys. Controlled Fusion **47**, 1817 (2005).

[22]T. Drouot, E. Gravier, T. Reveille, M. Sarrat, M. Collard, P. Bertrand, T. Cartier-Michaud, P. Ghendrih, Y. Sarazin, and X. Garbet, Phys. Plasmas **22**, 082302 (2015).

[23]T. Drouot, E. Gravier, T. Reveille, and M. Collard, Phys. Plasmas **22**, 102309 (2015).

[24]T. Cartier-Michaud, P. Ghendrih, V. Grandgirard, and G. Latu, ESAIM: Proc. **43**, 274 (2013).

[25]T. Cartier-Michaud, P. Ghendrih, Y. Sarazin, G. Dif-Pradalier, T. Drouot, D. Estève, X. Garbet, V. Grandgirard, G. Latu, C. Norscini, and C. Passeron, J. Phys.: Conf. Ser. **561**, 012003 (2014).

[26]A. Ghizzo, D. Del Sarto, X. Garbet, and Y. Sarazin, Phys. Plasmas **17**, 092501 (2010).

[27]E. Gravier, M. Lesur, T. Reveille, and T. Drouot, Phys. Plasmas **23**, 092507 (2016).

[28]E. Gravier, M. Lesur, T. Reveille, T. Drouot, and J. Médina, Nucl. Fusion **57**, 124001 (2017).

[29]B. Kadomtsev and O. P. Pogutse, Reviews of Plasma Physics (Consultants Bureau, New-York, 1970), Vol. 5, p. 249.

[30]X. Garbet, Y. Idomura, L. Villard, and T. H. Watanabe, "Gyrokinetic simulations of turbulent transport," Nucl. Fusion **50**, 043002 (2010).

[31]J. C. Lagarias, J. A. Reeds, M. H. Wright, and P. E. Wright, SIAM J. Optimization **9**, 112 (1998).

[32]E. Sonnendrucker, J. Roche, P. Bertrand, and A. Ghizzo, J. Comp. Phys. **149**, 201 (1999).

[33]M. Lesur, T. Cartier-Michaud, T. Drouot, P. H. Diamond, Y. Kosuga, T. Reveille, E. Gravier, X. Garbet, S.-I. Itoh, and K. Itoh, Phys. Plasmas **24**, 012511 (2017).

[34]J. Médina, M. Lesur, E. Gravier, T. Reveille, M. Idouakass, T. Drouot, P. Bertrand, T. Cartier-Michaud, X. Garbet, and P. H. Diamond, Phys. Plasmas **25**, 122304 (2018).